*photonics*

MDPI

*Article*

# Average BER Performance Estimation of Relayed THz Links with Losses, Molecular Attenuation, Adverse Weather Conditions, Turbulence and Generalized Pointing Errors

**George K. Varotsos [1], Konstantinos Aidinis [2,3] and Hector E. Nistazakis [1,*]**

[1] Section of Electronic Physics and Systems, Department of Physics, National and Kapodistrian University of Athens, 15784 Athens, Greece
[2] Department of Electrical and Computer Engineering, Ajman University, Ajman P.O. Box 346, United Arab Emirates
[3] Centre of Medical and Bio-Allied Health Sciences Research (CMBHSR), Ajman University, Ajman P.O. Box 346, United Arab Emirates
* Correspondence: enistaz@phys.uoa.gr; Tel.: +30-210-7276710

**Abstract:** In recent years, the THz frequency band (0.3 THz–10 THz) has attracted an increasing research interest for the realization of emerging high-speed wireless communication links. Nevertheless, the propagation of THz signals through the atmospheric channel is primarily subjected to signal attenuation due to free space path loss (FSPL), water vapor, adverse weather conditions along with atmospheric turbulence-induced and misalignment-induced scintillations. Therefore, in this work, a multi-hop line-of-sight THz system that utilizes serially connected decode-and-forward relays is proposed to extend the total THz coverage distance under the presence of fog, rain or clear weather conditions, as well as water vapor, atmospheric turbulence, non-zero boresight pointing errors and FSPL. Under these circumstances, an average bit error rate (ABER) analysis is performed. In this context, novel closed-form ABER expressions are derived. Their analytical results demonstrate the influence of each of the above limiting factors as well as their joint impact on the ABER performance. Finally, the feasibility of extending the total THz link distance through multi-hop relaying configurations is also evaluated.

**Keywords:** terahertz; atmospheric turbulence; attenuation; rain; fog; free space path loss; non-zero boresight pointing errors; average BER; relays



**Citation:** Varotsos, G.K.; Aidinis, K.; Nistazakis, H.E. Average BER Performance Estimation of Relayed THz Links with Losses, Molecular Attenuation, Adverse Weather Conditions, Turbulence and Generalized Pointing Errors. *Photonics* **2022**, *9*, 671. https://doi.org/10.3390/photonics9100671

Received: 1 August 2022
Accepted: 15 September 2022
Published: 20 September 2022



## 1. Introduction

In recent years, the dramatic increase in the data traffic carried by telecommunication networks due to the continuous emergence of new high bandwidth services, smart devices and variable sophisticated applications has generated a significant spectrum congestion with the existing radio frequency (RF) systems. Initially, optical fiber systems provided the means to increase the amount of data to be transported. Despite their success, their installation is not always an easy, flexible or even viable task, for they cannot provide wireless connectivity and solve the last mile bottleneck problem. Complementing the existing wireless RF solutions, optical wireless communications (OWCs), commonly known as free space optical communications (FSOs) which mainly operate in the infrared (IR), visible light and ultra-violet bands, as well asmillimeter wave (MMW) communications that operate within 30–300 GHz have been initially developed [1–4]. Even more recently, the impressive advances in both wireless communication devices and high-directional antenna design technologies have paved the way to the exploitation of terahertz bands that areat the cross-section of the higher end of microwaves and the lower end of optical frequency bands, and thus, it can offer their distinct advantages [5]. Indeed, in comparison with MMW communication links, terahertz (THz) links achieve increasing capacities owing

to their larger atmospheric transmission window [6–8]. This is very critical since the sixth generation (6G) per user bit rate is expected to be 1 Tb/s in different fields of application, which the existing MMW links for 5G cannot accommodate, contrary to the emerging THz links which have the potential to reach such demands [5,9]. Moreover, potential applications of THz links also include virtual reality, augmented reality, holographic projection in 6G wireless communication, terabit wireless personal area networks, terabit wireless local area networks, cellular networks, transmission of high-definition television (HDTV) signals with low latency, wireless back-haul for data and voice communications, wireless extensions of broadband access to fiber optical networks to address the last-mile problem, machine-to-machine communications among sensor networks and critical biomedical applications such as health monitoring systems [5,7,9,10]. Additionally, THz outperforms MMW in terms of unregulated frequency spectrum, higher security level, lower transmitted power as well as higher directional information-bearing beams [10]. At the other side of the spectrum, when compared to IR FSO links, THz links are much less vulnerable to signal scintillations and signal attenuation under the presence of dust, clouds or atmospheric turbulence [11–14]. Likewise, THz links do not suffer from the stronger ambient infrared noise, whereas THz power transmissions are not constrained by eye-safety infrared emission power limits.

Nevertheless, rain attenuates THz radiation to a greater degree, which is a critical natural obstacle for THz deployment [15–17]. In this respect, the major limiting factor for the performance of THz links has been reported to be the THz signal attenuation due to humid air that results from molecular absorption mainly due to the presence of water vapor, and to a much lesser degree due to the presence of oxygen [18]. Apart from attenuation due to weather conditions and molecular absorption, the inevitable transmitted energy distribution over a large area, as the emitted THz signal is propagating towards the receiver side, brings about the attenuation due to FSPL. Thus, this unavoidable loss always exists and further degrades the THz links' performance [19].

Additionally, even in a clear sky temperature, pressure inhomogeneities bring about random variations of the refractive index along the atmospheric channel, which give rise to the atmospheric turbulence effect. The latter is a complex effect that generates the so-called scintillation effect which results, in turn, in rapid fluctuations of the intensity of the signal at the receiver side, analogous to fading in RF systems [2,20–23]. Although THz transmissions are generally less vulnerable to atmospheric turbulence than FSO transmissions, turbulence-induced THz performance degradations are not negligible and should be taken into consideration, especially in a long-path propagation that emerging THz links are expected to accommodate [19].

Another concern in THz links is the pointing errors effect that mainly arises from building sway. Thermal expansion, dynamic wind loads as well as weak earthquakes bring about the sway of high-rise building structures where THz terminals are usually placed. The latter results in random vibrations of the transmitted information-bearing beam and consequently in stochastic misalignments between transmitter and receiver antenna terminals. These unavoidable misalignments, which are commonly known as pointing errors, generate random intensity variations of the propagated signal arriving at the receiver aperture which strongly degrades the THz performance and availability [24–27]. More precisely, pointing errors consist of both boresight and jitter components [22]. The former is the fixed displacement between the beam and the detector center, while the latter is the random offset of the beam center at the detector plane [28].

In short, while line of sight (LOS) THz links exhibit concrete advantages that make them a prime candidate to reach the growing demands of the emerging wireless communications, their deployment is impaired by attenuations due to weather effects and especially rain, attenuations due to molecular absorption and especially water vapor, attenuations due to FSPL, atmospheric turbulence and pointing errors. It therefore becomes evident that a generalized LOS channel model that evaluates the joint impact of all the above detrimental effects could be a very useful tool for the design and the establishment of such LOS THz links. Still, this research gap remains in the open technical literature.

Specifically, a good approximation for the attenuation of the lower frequency band of THz waves (0.1–1 THz) due to molecular absorption is the ITU-R model [19]. In this respect, the authors of [29,30], by using time domain spectroscopy, investigated attenuation due to water vapor from 0.2–2 THz, while in [18] they confirmed four transparent windows at 0.41 THz, 0.46 THz, 0.68 THz and 0.85 THz. Recently, attenuation due to water vapor in the presence of dry air has been assessed for practical outdoor THz links in [31]. Additionally, based on the model proposed in [32], the authors of [33] proposed an alternative channel model including path loss, transceiver parameters and molecular absorption. The above results demonstrate that in terms of molecular attenuation, attenuation due to water vapor is more significant than attenuation due to oxygen within the frequency regions in which emerging THz links operate. Attenuation due to fog, cloud or rain has been evaluated through the Laser Environmental Effects Definition and Reference (LEEDR) computation tool in [34] as well as through a theoretical framework and/or experimentally in a laboratory or a real outdoor environment in [5,11–13,15–17,35–37]. Apart from the feasibility of establishing realistic THz links, their findings reveal that experimental results are in good agreement with the predicted attenuation due to weather effects, with rain being the most destructive effect for the emerging THz transmissions. Moreover, it is highlighted that attenuation due to weather effects must be taken into consideration, especially for longer THz link lengths, while THz outperforms FSOs under fog conditions and thus THz can be a promising alternative for many wireless applications in fog. Additionally, the atmospheric turbulence effect over THz link channels has been experimentally studied in a laboratory environment in [14,38], as well as theoretically in [39], where in the authors estimated turbulence-induced THz scintillation through the estimation of the scintillation index metric. Their results mainly indicate that although atmospheric turbulence is less significant for THz compared to FSO channels, it should not be neglected, especially for the longer propagation distances that modern THz links can support. Thus, stochastic distribution models are needed to emulate these turbulence-induced THz signal scintillations. In this respect, the authors of [19,40] recently introduced in the THz area the well-known (from the FSOs open literature) Gamma–Gamma, Lognormal and Exponentiated Weibull turbulence distribution models, while also even more recently the authors of [41] proposed the Gamma distribution turbulence model as a simplified alternative to the Lognormal distribution for weak-to-moderate THz turbulence conditions. Furthermore, the influence of THz beams misalignment between transmitter and receiver terminals was initially considered as a part of the shadowing effect in [42], while it was later evaluated in [43,44] through deterministic models. Consequently, these works could not incorporate the stochastic nature of pointing errors. Their stochastic impact for THz links has been first evaluated by the authors of [27,45,46], relying mainly on the well-known zero boresight pointing error model which was first proposed in [24] for FSO links. In this context, the authors of [19,40] and then the authors of [41] studied the joint impact of turbulence and zero boresight stochastic pointing errors on THz link performance for different turbulence distributions. Nevertheless, in terms of the impact of the more realistic non-zero boresight (NZB) stochastic pointing errors, there is still a research gap in the THz literature. Additionally, the use of relays has been recently introduced in the THz band in [47,48] and then in [49–54], which demonstrate the feasibility of establishing relay-assisted THz links to address several effects that mitigate THz performance and availability.

Motivated by the above and inspired also by several multi-hop FSO relaying configurations that have been reported to successfully enhance the total propagation distance [22,23,55–58], in this work a multi-hop THz system is investigated over different channel and link characteristics that incorporate for the first time the combined impact of all the major effects described above. The evaluation of the impact of each factor as well as their joint influence on the THz system's performance is performed by means of the crucial ABER performance metric. Therefore, the first key contribution of this paper is the establishment of a THz system and channel model including atmospheric turbulence, stochastic ZB or NZB pointing errors, attenuation due to FSPL, attenuation due to molec-

ular absorption that arises especially from water vapor and attenuation due to weather conditions and especially due to the presence of rain or fog. It is also remarkable that the proposed system and channel model include different critical design parameters, such as the selected operational THz frequency value, the transmitter and receiver antennas' gain and the number of intermediate relay nodes along with the total distance of the multi-hop THz link. Based on the proposed model and after performing an ABER analysis, novel closed-form ABER expressions are derived. To the best of the authors' knowledge, the extracted ABER expressions are the first closed-form ABER expressions that incorporate all the above major effects and design parameters in the open technical THz literature. In this context, proper analytical results are presented for different multi-hop THz link configurations that reveal the impact of each of these performance factors along with their joint impact. Consequently, the proposed analysis can be a very useful tool for the design of the emerging long-path THz links.

## 2. System and Channel Model

### *2.1. Basic Principles of the Investigated THz System*

The typical multi-hop LOS THz system under consideration comprises the transmitter node, the receiver node and the $N$-1 serially connected decode-and-forward (DF) relay nodes along the propagation channel, with $N \geq 1$. Therefore, $N$ distinct intermediate THz links, commonly known as hops, are created along the total propagation path. Each relay node decodes the signal after direct detection, remodulates it and retransmits it to the next relay node, provided that it exceeds a given appropriate decoding intensity threshold. This process continues until the source's data arrives at the receiver destination node [56]. Without loss of generality, these intermediate links can be assumed to be of equal length. Additionally, the investigated system is considered to employ the On-Off Keying (OOK) modulation format which is commonly utilized in both commercial and industrial fields, mainly due its simplicity among the rest of the alternative modulation schemes. Under these assumptions, the THz signal that arrives at the $n$-th node, where $1 \leq n \leq N$, is expressed as:

$$y_n = h_n x_{n-1} + n_n \tag{1}$$

where $h_n$ is the total corresponding channel state due to atmospheric turbulence, total attenuation and generalized pointing errors, $x_{n-1} = \{0 \text{ or } 2P_t\}$ is the corresponding emitted information signal according to the OOK modulation format with $P_t$ being the average transmitted signal power and $n_n$ represents the corresponding additive Gaussian white noise with variance $\sigma_n^2$ [19].

### *2.2. Total Attenuation*

The total channel coefficient for each THz hop can be written as

$$h_n = h_{l,n} h_{p,n} h_{a,n}, \tag{2}$$

where $h_{l,n}$, $h_{p,n}$ and $h_{a,n}$ denote the THz signal intensity due to the deterministic total attenuation, generalized pointing errors and atmospheric turbulence, respectively [21,24,41].

The above deterministic total attenuation factor can be expressed in turn as

$$h_{l,n} = h_{fl,n} h_{vl,n} h_{wl,n}, \tag{3}$$

where $h_{fl,n}$, $h_{vl,n}$ and $h_{wl,n}$ denote the attenuation due to FSPL, the molecular attenuation due to the water vapor and the attenuation caused by the weather effects, respectively. It should be clarified here that the latter attenuation factor obtains different values in case of fog and rain as it will be explained below. Additionally, it should be noted that $h_{wl,n} = 1$ in case of clear weather conditions. Indeed, in clear weather conditions, Equation (3) reduces to $h_{l,n} = h_{fl,n} h_{vl,n}$ as it was reported in [19,27,41], where the presence of adverse weather effects was not taken into consideration.

In more detail, the deterministic attenuation factor due to FSPL is obtained according to Friis equation as seen in [45]

$$h_{fl,n} = c\sqrt{G_t G_r}(4\pi f_n z_n)^{-1}, \tag{4}$$

where $c$ is the speed of the light in the free space, $f_n$ represents the frequency of the information-bearing THz carrier wave which propagates along the $n$-th link, $z_n$ denotes the $n$-th link length and $G_t$, $G_r$ are standing for the transmission and reception antenna gains of the corresponding nodes, respectively.

Additionally, the molecular attenuation term due to the propagating signal's absorption along the $n$-th hop can be obtained according to the well-known Beer–Lambert Law as [11]:

$$h_{vl,n} = exp(-a_{v,n} z_n), \tag{5}$$

with $a_{v,n}$ being the attenuation coefficient in $\mathrm{m}^{-1}$ while the propagation distance along the $n$-th THz hop, $z_n$, is expressed in meters. Bearing in mind that water vapor dominates in terms of THz attenuation over gaseous oxygen and any other species of gases as well as those at lower atmospheric altitudes where THz links are located, water vapor remains a major limiting factor in determining the maximum link distance, the maximum THz frequency of the link and the link performance [8,10,59], we have, without loss of generality, set $a_{v,n}$ as the attenuation coefficient due to water vapor which at $T_0 = 20$ °C surface temperature and for $f \leq 350$ GHz is obtained as [60]:

$$a_{v,l}\left(\frac{\mathrm{dB}}{\mathrm{km}}\right) = \left[0.067 + \frac{2.4}{(f_n - 22.3)^2 + 6.6} + \frac{7.33}{(f_n - 183.5)^2 + 5} + \frac{4.4}{(f_n - 323.8)^2 + 10}\right] f_n^2 \rho_n \times 10^{-4} \tag{6}$$

where the operation frequency $f_n$ is now expressed in GHz, while $\rho_n$ represents the water vapor concentration in $\mathrm{g/m}^3$ along the corresponding channel. It should be mentioned here that as the surface temperature decreases, the attenuation coefficient is expected to increase by about 1% per degree Celsius, and vice versa [60].

Similarly, the attenuation factor due to weather conditions prevailing along the $n$-th hop can be obtained as

$$h_{wl,n} = exp(-a_{w,n} z_n), \tag{7}$$

with $a_{w,n}$ being the attenuation coefficient for the specific weather effect which is usually experimentally measured in $\mathrm{km}^{-1}$, while the propagation distance along the $n$-th THz hop, $z_n$, is expressed in km. Additionally, it should be clarified that the attenuation due to any weather condition such as rain or fog can be added to both attenuation due to FSPL and the molecular attenuation due to water vapor [19]. Consequently, in this work the total attenuation due to water vapor, rain or fog and FSPL will be jointly considered by properly utilizing the above attenuation expressions.

### *2.3. Atmospheric Turbulence Model*

Even in clear weather conditions, the atmospheric turbulence effect is observed. In fact, solar radiation absorbed by the Earth's surface makes the air around the Earth's surface warmer than that at higher altitudes. This layer of warmer air becomes less dense and rises to mix turbulently with the surrounding cooler air, causing the air temperature to fluctuate randomly. These random temperature variations lead to corresponding refractive index fluctuations and thus, inhomogeneities caused by turbulence can be considered as discrete cells, or eddies of different temperatures, acting like refractive prisms of different sizes and refractive indices. The interaction between THz propagating wavelengths and turbulent medium generates random phase and amplitude variations of the received signal, which results in the performance degradation of the link. Consequently, atmospheric turbulence is a very complex stochastic effect which hinders the propagation of the information-bearing beam and causes the so-called scintillation effect which results, in turn, in random

temporal and spatial fluctuations of the received signal intensity, analogous to fading in RF systems [2,20,40,61,62]. Considering therefore that this effect brings about continuous and very rapid fluctuations on the intensity of the signal that arrives at the receiver's side, it should be mainly investigated through statistical methods and processes. The selection of the appropriate model is mainly determined by the strength of the turbulence effect along the propagation path. In this work, turbulence-induced scintillations are described by the Gamma–Gamma distribution model [21,24,26,54,57,58,63,64], which has been widely used in the FSOs area and more recently in the THz regime [19,40] as a very accurate model for weak-to-strong turbulent conditions. According to the well-known Gamma–Gamma turbulence model, which was first proposed in [65], the PDF of the positive random variable $h_{a,n}$ is obtained as

$$\begin{aligned} f_{h_{a,n}}(h_{a,n}) &= \frac{2(\alpha_n\beta_n)^{\frac{\alpha_n+\beta_n}{2}}}{\Gamma(\alpha_n)\Gamma(\beta_n)} h_{a,n}^{\frac{\alpha_n+\beta_n}{2}-1} \\ &\times K_{\alpha_n-\beta_n}\left(2\sqrt{\alpha_n\beta_n h_{a,n}}\right), \end{aligned} \tag{8}$$

with $\Gamma(.)$ representing the gamma function [66], Equation (8.310.1), $K_\nu(.)$ denoting the $\nu$-th order modified Bessel function of the second kind [66], Equation (8.432.2), while the parameters $\alpha_n$ and $\beta_n$ can be directly related to the $n$-th turbulent channel along with the link's parameters, as described in [63]:

$$\begin{aligned} \alpha_n &= \left[ exp\left( \frac{0.49\delta_n^2}{\left(1 + 0.18d_n^2 + 0.56\delta_n^{\frac{12}{5}}\right)^{\frac{7}{6}}} \right) - 1 \right]^{-1} \\ \beta_n &= \left[ exp\left( \frac{0.51\delta_n^2\left(1 + 0.69\delta_n^{12/5}\right)^{-5/6}}{\left(1 + 0.9d_n^2 + 0.62d_n^2\delta_n^{12/5}\right)^{\frac{5}{6}}} \right) - 1 \right]^{-1}, \end{aligned} \tag{9}$$

where $d_n = 0.5D_n\sqrt{2\pi\lambda_n^{-1}z_n^{-1}}$, with $D_n$ standing for the receiver's aperture diameter and $\lambda_n = c/f_n$ being the operational wavelength, while the parameter $\delta^2$ denotes the Rytov variance for which the spherical wave propagation in a horizontal path is obtained as [67,68]:

$$\delta_n^2 = 0.5C_n^2 k_n^{\frac{7}{6}} z_n^{\frac{11}{6}}, \tag{10}$$

with $k_n = 2\pi/\lambda_n$ being the wavenumber and $C_n^2$ representing the refractive index structure parameter which is proportional to the atmospheric turbulence strength [67,68]. Consequently, the Rytov variance is a metric of turbulence-induced scintillations, while also it becomes evident from Equation (10) that atmospheric turbulence is a wavelength-dependent and especially a distance-dependent effect. The latter gives an early indication that while it has been proved in [14,15] that THz radiation is less vulnerable to atmospheric turbulence-induced scintillations than IR radiation, the atmospheric turbulence effect should not be neglected for the design of modern and future THz links which are expected to cover longer propagation distances.

### *2.4. Generalized Pointing Errors Model*

In order to accurately describe the stochastic nature of the pointing errors effect including the boresight component, the general and realistic Beckmann distribution statistical distribution model was used. The PDF of the $n$-th radial displacement at the receiver $R_n$, according to the Beckmann model which takes into consideration the influence of beam

width, detector size, the different jitter for elevation and horizontal displacement as well as the effect of pointing errors with boresight, is obtained as described in [22,28,69]

$$f_{R_n}(R_n) = \frac{R_n}{2\pi\sigma_{x,n}\sigma_{y,n}} \times \int_0^{2\pi} exp\left(-\frac{(R_n\cos\zeta_n-\mu_{x,n})^2}{2\sigma_{x,n}^2} - \frac{\left(R_n\sin\zeta_n-\mu_{y,n}\right)^2}{2\sigma_{y,n}^2}\right)d\zeta_n, \tag{11}$$

where $\zeta_n$ is the divergence angle describing the increase in the beam radius at the receiver with a distance $z_n$ from the transmitter, whereas the beam width could be approximated as $w_{z,n} \approx \zeta_n z_n$ for relatively long propagation distances. Additionally, $R_n = \sqrt{R_{x,n}^2 + R_{y,n}^2}$ where $R_{x,n}^2$ and $R_{y,n}^2$ denote the offsets along the horizontal and elevation axes at the detector plane, respectively. In this context, the random variables $R_{x,n}$ and $R_{y,n}$ are considered as nonzero mean Gaussian random variables, i.e., $R_{x,n} \sim N\left(\mu_{x,n}, \sigma_{x,n}^2\right)$ and $R_{y,n} \sim N\left(\mu_{y,n}, \sigma_{y,n}^2\right)$ with $\mu_{x,n}$ and $\mu_{y,n}$ representing the mean values, whereas $\sigma_{x,n}$ and $\sigma_{y,n}$ are the standard deviations for horizontal and elevation displacements, respectively. According to the analysis which has been performed in [69], the Beckmann distribution above can be accurately simplified through a modified Rayleigh distribution as

$$f_{R_n}(R_n) = \frac{R_n}{\sigma_{mod,n}^2} exp\left(-\frac{R_n^2}{2\sigma_{mod,n}^2}\right), R_n \geq 0, \tag{12}$$

with $\sigma_{mod,n}$ being the joint standard deviation of $\sigma_{x,n}$ and $\sigma_{y,n}$ for the $n$-th hop, expressed as follows [69],

$$\sigma_{mod,n}^2 = \left(\frac{3\mu_{x,n}^2\sigma_{x,n}^4 + 3\mu_{y,n}^2\sigma_{y,n}^4 + \sigma_{x,n}^6 + \sigma_{y,n}^6}{2}\right)^{\frac{1}{3}} \tag{13}$$

Therefore, according to [69], the PDF of the random variable $h_{p,n}$ can be written as

$$f_{h_{p,n}}(h_{p,n}) = \frac{\psi_n^2}{(A_{0,n}g_n)^{\psi_n^2}} h_{p,n}^{\psi_n^2-1}, 0 \leq h_{p,n} \leq g_n A_{0,n}, \tag{14}$$

where $\psi_n = w_{z,eq,n}/2\sigma_{mod,n}$ refers to the total amount of the pointing mismatch at the $n$-th receiver aperture. Indeed, larger values of $\psi_n$ denote weaker generalized pointing errors, and conversely, smaller values of $\psi_n$ correspond to a stronger total amount of pointing mismatch [22]. Similarly, $\psi_{x,n} = w_{z,eq,n}/2\sigma_{x,n}$ and $\psi_{y,n} = w_{z,eq,n}/2\sigma_{y,n}$ indicate the specific generalized misalignment strengths along the horizontal and elevation axis, respectively. It is worth noting here that $w_{z,eq,n} = \left[\sqrt{\pi}\text{erf}(v_n)w_{z,n}^2/2v_n exp\left(-v_n^2\right)\right]^{1/2}$, with $A_{0,n} = \text{erf}^2(v_n)$ representing the fraction of the collected power at $r_n = 0$ , with erf(.) standing for the error function [70], Equation (7.1.1), and $r_n$ being the radius of the $n$-th receiver aperture, while $v_n = \sqrt{\pi}r_n/\sqrt{2}w_{n,z}$, and $w_{n,z}$ standing for the corresponding beam waist on the receiver plane at propagating distance $z_n$ [19,24]. Additionally, the parameter $g_n = exp\left(\frac{1}{\psi_n^2} - \frac{1}{2\psi_{x,n}^2} - \frac{1}{2\psi_{y,n}^2} - \frac{\mu_{x,n}^2}{2\sigma_{x,n}^2\psi_{x,n}^2} - \frac{\mu_{y,n}^2}{2\sigma_{y,n}^2\psi_{y,n}^2}\right)$ determines the presence of ZB or NZB pointing errors. Indeed, when the boresight displacement at the $n$-th hop $s_n = \sqrt{\mu_{x,n}^2 + \mu_{y,n}^2}$ is equal to zero, i.e., $\mu_{x,n} = \mu_{y,n} = 0$ , and $\sigma_{x,n} = \sigma_{y,n}$ then $g_n = 1$. In other words, when $g_n = 1$, we have only ZB pointing errors and more specifically the Beckmann model is reduced to a Rayleigh distribution with $s_n = 0$, and thus, expression (12) is simplified into [24], Equation (10) while also (14) reduces to [24], Equation (11).

### *2.5. Joint Impact of Attenuation, Turbulence and NZB Pointing Errors*

The joint PDF of the total channel state for each hop can be deduced from the integral below

$$f_{h_n}(h_n) = \int f_{h_n|h_{a,n}}(h_n|h_{a,n}) f_{h_{a,n}}(h_{a,n}) dh_{a,n}, \tag{15}$$

where $f_{h_n|h_{a,n}}(h_n|h_{a,n})$ stands for the conditional probability of $h_n$ given $h_{a,n}$ [67]. The latter can be expressed as [57]

$$\begin{aligned} f_{h_n|h_{a,n}}(h_n|h_{a,n}) &= \frac{dF_{h_{p,n}}(h_n|h_{a,n}h_{l,n})}{dh_n} = \frac{\psi_n^2}{(A_{0,n}g_n)^{\psi_n^2} h_{a,n}h_{l,n}} \left(\frac{h_n}{h_{a,n}h_{l,n}}\right)^{\psi_n^2-1}, \; 0 \le h_n \\ &\le A_{0,n}g_n h_{l,n}, \end{aligned} \tag{16}$$

where $F(.)$ stands for the cumulative distribution function (CDF).

By substituting (8) and (16) by (15) and by utilizing the analysis performed in [63], we obtain

$$\begin{aligned} f_{h_n}(h_n) &= \frac{\alpha_n \beta_n \psi_n^2}{A_{0,n}g_n h_{l,n} \Gamma(\alpha_n)\Gamma(\beta_n)} \\ &\times G_{1,3}^{3,0}\left( \frac{\alpha_n \beta_n h_n}{A_{0,n}g_n h_{l,n}} \middle| \begin{matrix} \psi_n^2 \\ \psi_n^2 - 1, \; \alpha_n - 1, \; \beta_n - 1 \end{matrix} \right), \end{aligned} \tag{17}$$

where $G_{p,q}^{m,n}(.)$ denotes the Meijer *G*-function, [71].

## 3. Average BER Estimation

### *3.1. On-Off Keying Modulation*

According to the On-Off keying (OOK) modulation format, the instantaneous BER for each hop can be obtained as described in [25]:

$$P_{e,n} = p_n(1) p_n(e|1) + p_n(0) p_n(e|0), \tag{18}$$

where $p_{\mathrm{n}}$ (0) and $p_{\mathrm{n}}$ (1) denote the probabilities of transmitting the bits "0" and "1", respectively, while $p_{\mathrm{n}}$ ($e$ |0) and $p_{\mathrm{n}}$ ($e$|1) are their corresponding conditional bit-error probabilities [2]. By assuming that $p_n(0) = p_n(1) = 1/2$ and $p_n(e|0) = p_n(e|1)$ we obtain [57]:

$$P_{e,n} = p_n(e|1) = p_n(e|0) = \frac{1}{2}\mathrm{erfc}\left(\frac{P_t h_n}{\sqrt{2}\sigma_n}\right), \tag{19}$$

where erfc(.) stands for the complementary error function [70], Equation (8.250.4).

The average BER for the $n$-th hop is defined as

$$P_{e,av,n} = \int_0^\infty f_{h_n}(h_n) P_{e,av,n} dh_n, \tag{20}$$

Consequently, by substituting (17) and (19) by (20), we obtain

$$\begin{aligned} P_{e,av,n} &= \frac{\alpha_n \beta_n \psi_n^2}{2A_{0,n}g_n h_{l,n} \Gamma(\alpha_n)\Gamma(\beta_n)} \\ &\times \int_0^\infty \mathrm{erfc}\left(\frac{P_t h_n}{\sqrt{2}\sigma_n}\right) G_{1,3}^{3,0}\left( \frac{\alpha_n \beta_n h_n}{A_{0,n}g_n h_{l,n}} \middle| \begin{matrix} \psi_n^2 \\ \psi_n^2 - 1, \alpha_n - 1, \; \beta_n - 1 \end{matrix} \right) dh_n \end{aligned} \tag{21}$$

In order to solve the integral of (20), we initially transform the above complementary error function in terms of Meijer G-function by utilizing [71], (03.04.26.0009.01). Next, by using [72], Equation (21), and after performing some mathematical manipulations, we obtain:

$$\begin{aligned} P_{e,av,n} &= \frac{2^{\alpha_n+\beta_n-4}\psi_n^2}{\sqrt{\pi^3}\Gamma(\alpha_n)\Gamma(\beta_n)} \\ &\times G_{7,4}^{2,6}\left( \frac{8P_t^2 A_{0,n}^2 g_n^2 h_{l,n}^2}{\sigma_n^2 a_n^2 \beta_n^2} \middle| \begin{matrix} 1, \frac{1-\psi_n^2}{2}, \frac{2-\psi_n^2}{2}, \frac{1-\alpha_n}{2}, \frac{2-\alpha_n}{2}, \frac{1-\beta_n}{2}, \frac{2-\beta_n}{2} \\ 0, \frac{1}{2}, -\frac{\psi_n^2}{2}, \frac{1-\psi_n^2}{2} \end{matrix} \right), \end{aligned} \tag{22}$$

By simplifying (22) through [71] (07.34.03.0002.01) and also considering (3) and $N_{0,n} = \sigma_n^2/2$, we eventually obtain

$$P_{e,av,n} = \frac{2^{\alpha_n+\beta_n-4}\psi_n^2}{\sqrt{\pi^3}\Gamma(\alpha_n)\Gamma(\beta_n)} \times G_{6,3}^{2,5}\left(\frac{16P_t^2h_{fl,n}^2h_{vl,n}^2h_{wl,n}^2}{N_{0,n}A_{0,n}^{-2}g_n^{-2}a_n^2\beta_n^2}\middle| \begin{matrix} 1, \frac{2-\psi_n^2}{2}, \frac{1-\alpha_n}{2}, \frac{2-\alpha_n}{2}, \frac{1-\beta_n}{2}, \frac{2-\beta_n}{2} \\ 0, \frac{1}{2}, -\frac{\psi_n^2}{2} \end{matrix}\right). \tag{23}$$

Thus, it becomes evident that the ABER for a THz link is obtained through (23) which incorporates atmospheric turbulence, NZB or ZB pointing errors, FSPL, attenuation due to water vapor along with attenuation due to weather conditions.

According to the analysis performed in [73], the total ABER for a multi-hop system is given by

$$P_{e,av,tot} = \sum_{i=1}^{N}\left[P_{e,av}(i)\prod_{j=i+1}^{N}(1-P_{e,av}(j))\right], \tag{24}$$

Therefore, considering the same single-hop ABER value $P_{e,av,n}$ in all $N$ hops of the system under investigation, the latter expression can be accurately written as

$$P_{e,av,tot} = \sum_{n=1}^{N}P_{e,av,n}\prod_{j=n+1}^{N}(1-2P_{e,av,n}), \tag{25}$$

or alternatively as described in [73]

$$P_{e,av,tot} = P_{e,av,n}\sum_{n=1}^{N}\prod_{j=n+1}^{N}(1-2P_{e,av,n}) = P_{e,av,n}\sum_{n=1}^{N}(1-2P_{e,av,n})^{N-n}. \tag{26}$$

Consequently, by substituting (23) by (25), we eventually obtain the total ABER for the examined THz multi-hop system as follows:

$$P_{e,av,tot} = \sum_{n=1}^{N}\Xi_n G_{6,3}^{2,5}\left(\frac{16P_t^2h_{fl,n}^2h_{vl,n}^2h_{wl,n}^2}{N_{0,n}A_{0,n}^{-2}g_n^{-2}a_n^2\beta_n^2}\middle| \begin{matrix} 1, \frac{2-\psi_n^2}{2}, \frac{1-\alpha_n}{2}, \frac{2-\alpha_n}{2}, \frac{1-\beta_n}{2}, \frac{2-\beta_n}{2} \\ 0, \frac{1}{2}, -\frac{\psi_n^2}{2} \end{matrix}\right) \times \prod_{j=n+1}^{N}\left(1-2\Xi_n G_{6,3}^{2,5}\left(\frac{16P_t^2h_{fl,n}^2h_{vl,n}^2h_{wl,n}^2}{N_{0,n}A_{0,n}^{-2}g_n^{-2}a_n^2\beta_n^2}\middle| \begin{matrix} 1, \frac{2-\psi_n^2}{2}, \frac{1-\alpha_n}{2}, \frac{2-\alpha_n}{2}, \frac{1-\beta_n}{2}, \frac{2-\beta_n}{2} \\ 0, \frac{1}{2}, -\frac{\psi_n^2}{2} \end{matrix}\right)\right), \tag{27}$$

where we have set $\Xi_n = \frac{2^{\alpha_n+\beta_n-4}\psi_n^2}{\sqrt{\pi^3}\Gamma(\alpha_n)\Gamma(\beta_n)}$.

Therefore, through (27), the total ABER for a multi-hop THz system is obtained, which mainly includes the impact of atmospheric turbulence, generalized pointing errors, number of hops, FSPL, attenuation due to water vapor along with attenuation due to weather conditions.

### *3.2. L-Symbol Pulse Amplitude Modulation Modulation*

It is worth mentioning that the analysis performed above can be extended to accommodate more complex modulation formants. An example is theL-symbol Pulse Amplitude Modulation ($L$-PAM) modulation format which has been proved to achieve spectral efficiency enhancements in the wider wireless communications field in comparison to OOK [74–76]. According to $L$-PAM, the information is encoded into $L$ different amplitudes, which represent the $L$ different symbols. Thus, considering in Equation (1) that $x_{n-1}$ is the corresponding $L$-PAM symbol amplitude, the instantaneous BER for the $L$-PAM signaling technique can be, correspondingly to Equation (19), obtained as described in [76]

$$P_{e,n,L-PAM} = \frac{L-1}{L\log_2 L}\mathrm{erfc}\left(\sqrt{\frac{P_t^2h_n^2\log_2 L}{2\sigma_n^2(L-1)^2}}\right). \tag{28}$$

Next, by following the analysis performed above and correspondingly to Equation (23), we obtain the ABER for each $L$-PAM THz hop as

$$P_{e,av,n,L-PAM} = \frac{2^{\alpha_n+\beta_n-3}\psi_n^2}{\sqrt{\pi^3}\Gamma(\alpha_n)\Gamma(\beta_n)}\frac{(L-1)}{(L\log_2 L)} \times G_{6,3}^{2,5}\left(\frac{16(\log_2 L)P_t^2 h_{fl,n}^2 h_{vl,n}^2 h_{wl,n}^2}{N_{0,n}A_{0,n}^{-2}g_n^{-2}a_n^2\beta_n^2}\middle| \begin{matrix} 1, \frac{2-\psi_n^2}{2}, \frac{1-\alpha_n}{2}, \frac{2-\alpha_n}{2}, \frac{1-\beta_n}{2}, \frac{2-\beta_n}{2} \\ 0, \frac{1}{2}, -\frac{\psi_n^2}{2} \end{matrix}\right). \quad (29)$$

Consequently, correspondingly to Equation (27), we eventually obtain the ABER for the total $L$-PAM THz multi-hop system as

$$P_{e,av,tot,L-PAM} = \sum_{n=1}^{N}\Phi_n G_{6,3}^{2,5}\left(\frac{16(\log_2 L)P_t^2 h_{fl,n}^2 h_{vl,n}^2 h_{wl,n}^2}{N_{0,n}A_{0,n}^{-2}g_n^{-2}a_n^2\beta_n^2}\middle| \begin{matrix} 1, \frac{2-\psi_n^2}{2}, \frac{1-\alpha_n}{2}, \frac{2-\alpha_n}{2}, \frac{1-\beta_n}{2}, \frac{2-\beta_n}{2} \\ 0, \frac{1}{2}, -\frac{\psi_n^2}{2} \end{matrix}\right) \times \prod_{j=n+1}^{N}\left(1-2\Phi_n G_{6,3}^{2,5}\left(\frac{16P_t^2 h_{fl,n}^2 h_{vl,n}^2 h_{wl,n}^2}{N_{0,n}A_{0,n}^{-2}g_n^{-2}a_n^2\beta_n^2}\middle| \begin{matrix} 1, \frac{2-\psi_n^2}{2}, \frac{1-\alpha_n}{2}, \frac{2-\alpha_n}{2}, \frac{1-\beta_n}{2}, \frac{2-\beta_n}{2} \\ 0, \frac{1}{2}, -\frac{\psi_n^2}{2} \end{matrix}\right)\right), \quad (30)$$

where we have set $\Phi_n = \frac{2^{\alpha_n+\beta_n-3}\psi_n^2}{\sqrt{\pi^3}\Gamma(\alpha_n)\Gamma(\beta_n)}\frac{(L-1)}{(L\log_2 L)}$. It is worth noting that when $L = 2$, Equation (29) reduces into Equation (23), and Equation (30) reduces into Equation (27). The latter indicates that 2-PAM is a special case equivalent to OOK.

## 4. Analytical Results

In this section, proper analytical results obtained by the derived closed-form expressions are presented. These results mainly aim to reveal the individual impact of each of the above-mentioned major impairments as well as their joint influence on the total ABER and the coverage area of a typical THz system which may employ multiple hops. In more detail, the THz system under investigation may consist of $N = \{1, 2, 3 \text{ or } 4\}$ hops. Each of the $n = 1, 2, ..N$ hops are assumed to have the same, equal to $z_n = 150$ m, link length. The refractive index structure parameter is assumed to be $C_n^2 = 5 \times 10^{-14}$ m$^{-2/3}$ for weak or $C_n^2 = 2.3 \times 10^{-9}$ m$^{-2/3}$ or strong turbulence, similarly to the experimental measurements in [14]. Additionally, the system may operate with frequency equal to $f = f_n = 0.3$ THz or $f = f_n = 0.35$ THz, while in terms of the antenna characteristics, they have either aperture radius $r_n = 0.15$ m with gain $G = G_t = G_r = 55$ dBi or aperture radius $r_n = 0.7$ m with gain $G = G_t = G_r = 70$ dBi [19]. Note that unless otherwise stated, the $f = f_n = 0.3$ THz and $r_n = 0.15$m with gain $G = G_t = G_r = 55$ dBi transmitter and receiver pair is utilized in the following figures and results. Such transceiver antennas can practically support up to several hundreds of meters propagation distances which is consistent with the THz hop length of the investigated system. Specifically, the selected antenna gain can be practically achieved by employing high-gain Cassegrain antennas which are commonly used in the THz frequency regime of the selected central frequency [27], while the 55dBi antennas are also already manufactured and tested with success [77]. Consequently, we have selected the above operation frequency values for the examined link because they are appropriate for the operation of the practically applicable transmitter and receiver antenna terminals mentioned above, while they also are within the proper frequency regime in which Equation (6) is valid. In terms of the stochastic influence of the generalized pointing errors, different practical boresight and jitter component values have been assumed for each hop transmission, i.e., $w_n/r_n$ =9 with $(\mu_{x,n}/r_n, \mu_{y,n}/r_n, \sigma_{x,n}/r_n, \sigma_{y,n}/r_n) = (0, 0, 5, 5)$ or $(0, 0, 6, 6)$ for weak-to-strong ZB pointing errors and $(\mu_{x,n}/r_n, \mu_{y,n}/r_n, \sigma_{x,n}/r_n, \sigma_{y,n}/r_n) = (1, 2, 5, 5)$ or $(1, 2, 6, 6)$ for weak-to-strong NZB pointing errors, respectively [69]. Furthermore, it is assumed that in accordance with the practical channel and environmental circumstances, the surface temperature is equal to 20 °C, the air pressure is equal to 1 atm, while $\rho = \rho_n = 7.5$ g/m$^3$ or $\rho = \rho_n = 10$ g/m$^3$ for moderate-to-strong molecular attenuation due to water vapor along each THz hop, respectively [19,27,60]. Regarding the impact of weather effects, with the exception of a

clear sky along the THz channel, two different and realistic scenarios are examined. More precisely, the impact of fog attenuation is determined by an additional attenuation factor $a_{w,n} = 0.6$ dB/km, while rain attenuation is determined, in turn, by an additional attenuation factor $a_{w,n} = 3$ dB/km at a precipitation rate of 2 mm/h [5,34], (Figure 1). It is worth noting that unless otherwise stated, clear weather conditions are assumed and OOK modulation is utilized. Finally, $\sigma_n = 10^{-7}$ A/Hz in all link configurations [19,41], while Monte Carlo simulations are marked below with solid dots, which have been generated by Matlab software for values lower than $10^{-6}$. In this way, we further validate the corresponding analytical results obtained.

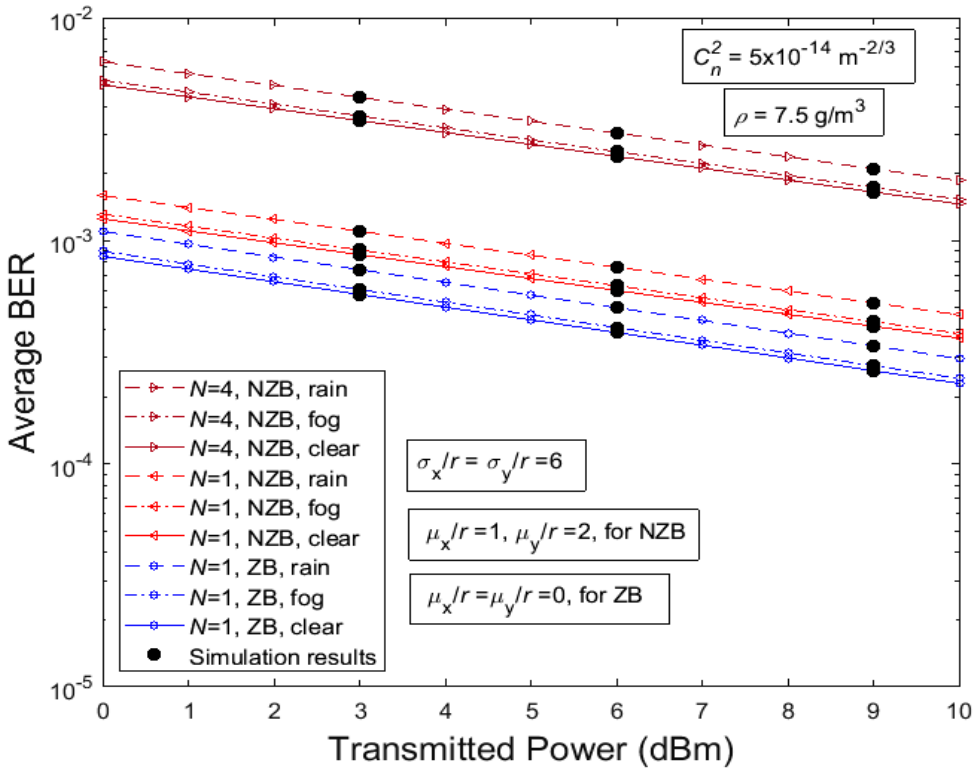


**Figure 1.** ABER vs. Transmitted power for single-hop and quad-hop THz link configurations under different weather conditions, weak turbulence, FSPL, moderate water vapor concentration and strong generalized pointing errors.

Figure 1 illustrates the ABER evolution for single-hop $(N = 1)$ or the quad-hop $(N = 4)$ LOS THz link configuration over a wide range of transmitted power through a weak turbulent channel with clear, rain or fog weather conditions and moderate air humidity along with the presence of FSPL and strong ZB or NZB pointing errors. It is depicted that for the same transmitted power and water vapor concentration values along with identical turbulence conditions, the weather effects and NZB pointing errors, the single-hop outperforms the quad-hop link configuration in terms of ABER. This is in accordance with other multi-hop configurations in the wider outdoor wireless communications literature [22,23,55], while it can be explained by the fact that most of the effects that affect the THz ABER performance such as FSPL, water vapor attenuation and atmospheric turbulence are distance-dependent. Thus, quadrupling the total THz coverage area becomes at the expense of this ABER performance degradation. Additionally, by focusing on single-hop configuration's ABER results, we can observe that higher corresponding ABER values are obtained when NZB pointing errors are considered instead of ZB pointing errors with the same spatial jitter. The latter indicates that as is the case with FSOs [2,28,67], the boresight component should not be neglected when stochastic pointing errors are estimated between THz transmitter and receiver terminals. Consequently, our initiative to include NZB pointing errors for THz links alike seems to be reasonable. Furthermore, for each

illustrated configuration, i.e., single-hop with ZB pointing errors, single-hop with NZB pointing errors and quad-hop with NZB pointing errors, three different weather scenarios are depicted, i.e., fog, rain or clear weather conditions. The performance comparison between them reveals that corresponding ABER values under rain are the largest. Likewise, ABER values under fog are slightly larger than their corresponding ABER values under clear weather conditions. This behavior indicates that rain is the most detrimental weather effect for THz signal transmissions while fog slightly aggravates the attenuation of the propagating THz signal. It is worth noting that the latter is qualitatively consistent with the experimental findings in [11,12,15–17]. It should be also recalled here that contrary to THz, the most detrimental weather effect for FSO transmissions is fog due to the comparable size of fog droplets with IR optical wavelengths [12,78], while conversely, FSO transmissions suffer only slightly from rain. This fact enables THz as a key complementary wireless technology to FSOs, paving the way for the development of hybrid FSO/THz links which will be able to efficiently operate in both rain and fog conditions. Finally, it is shown that higher transmitted power values lead to lower ABER values, as it was expected.

Figure 2 illustrates the ABER evolution for single-hop ($N$ =1) or the quad-hop ($N$ =4) LOS THz link configuration over a wide range of transmitted power through the same weak turbulence, FSPL, weather and air humidity conditions, but along with the presence of weak ZB or NZB pointing errors this time. The ABER qualitative behavior of Figure 2 is very similar to the one of Figure 1, which further enhances the accuracy of the analysis performed along with the conclusions discussed above. Nevertheless, all the ABER values from Figure 2 are lower than their corresponding ABER values from Figure 1, owing to the weaker amount of pointing mismatch which is assumed in the corresponding configurations of Figure 2. It is also worth noting that the detrimental impact of boresight component is now becoming more evident due to the lower spatial jitter values. Even for larger spatial jitter values, however, the boresight should be taken into consideration for the design of THz links, as indicated in Figure 1. Consequently, the performance comparison between the first two figures mainly reveals the impact of generalized pointing errors on the ABER performance of single-hop or multi-hop THz systems.

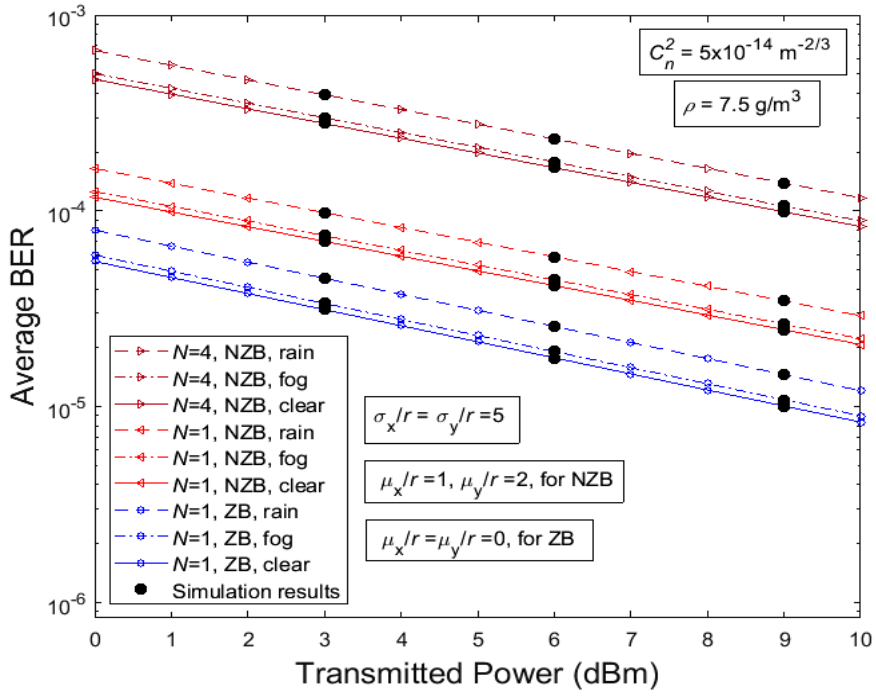


**Figure 2.** ABER vs. transmitted power for single-hop and quad-hop THz link configurations under different weather conditions, weak turbulence, FSPL, moderate water vapor concentration and weak generalized pointing errors.

Figure 3 illustrates the ABER evolution for the dual-hop LOS THz link configuration over a wide range of transmitted power through weak-to-strong atmospheric turbulence, weak ZB pointing errors, different transceiver antenna gains, clear weather along with moderate-to-high air humidity conditions. For the same transceiver gain of $G = 55$ dBi along with the same amount of pointing mismatch, it is highlighted that the impact of stronger water vapor concentrations along with stronger atmospheric turbulence significantly degrade the total THz ABER performance. It is also highlighted that especially for low transmitted power values, the impact of attenuation due to water vapor dominates. In fact, the worst-case scenario in Figure 3 is that represented by the blue solid line. Although there is a performance improvement as turbulence becomes weaker (blue dashed line),a better performance improvement can be observed when attenuation due to water vapor becomes weaker (red solid line) instead of turbulence. Consequently, it is demonstrated that the detrimental impact of attenuation due to water vapor is more important than the impact of turbulence-induced scintillations on the THz outage performance. The latter is qualitatively consistent with the experimental results in [11,14] that highlight that the atmospheric turbulence-induced scintillations are much less detrimental for THz links than molecular attenuation. Additionally, Figure 3 illustrates the potential of the utilization of more effective transceiver antennas of a higher gain $G = 70$ dBi, in an attempt to overcome turbulence, pointing errors and especially, high water vapor concentrations. Once again, these depicted outage performance improvements are qualitatively in accordance with the corresponding results obtained in several works.

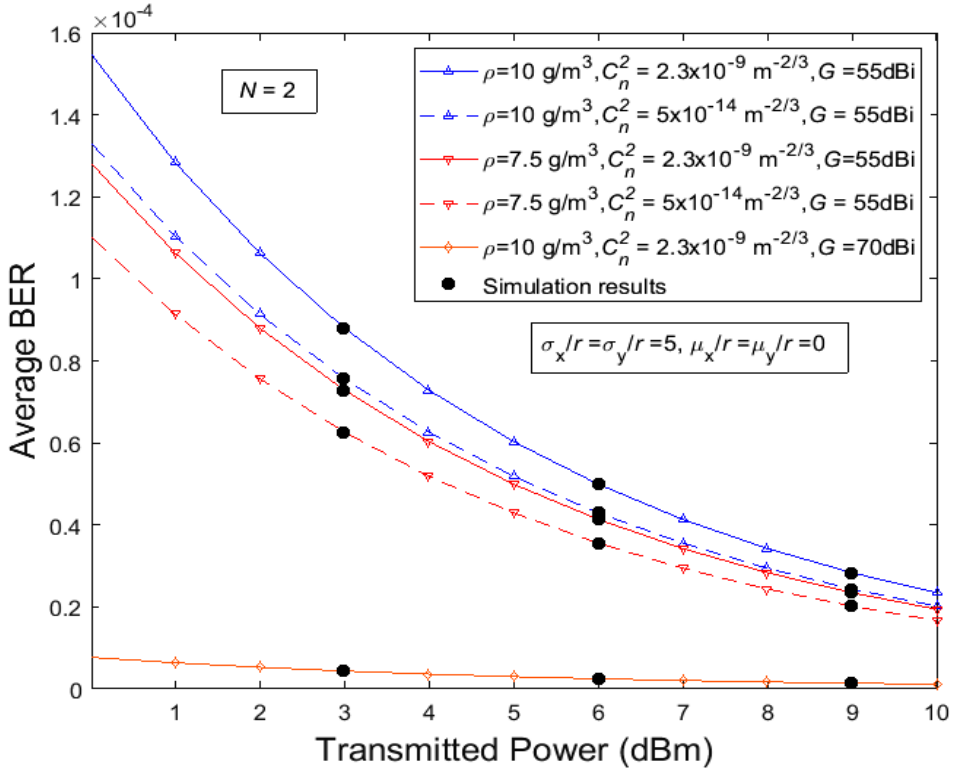


**Figure 3.** ABER vs. transmitted power for a dual-hop THz link configuration with different antenna gains, weak-to-strong turbulence, moderate-to-high water vapor concentrations and weak ZB pointing errors.

Figure 4 shows the ABER evolution for the triple-hop LOS THz link configuration over a wide range of transmitted power through strong atmospheric turbulence, strong NZB pointing errors, different operation frequencies, clear weather along with moderate-to-high air humidity conditions. It becomes evident from the illustrated results that even for strong joint turbulence and generalized pointing errors, the impact of THz signal's attenuation due to water vapor still drastically increases the total ABER of the system. Additionally,

it is highlighted that further significant ABER performance degradations are observed by increasing the operational frequency from $f = 0.3$ THz to $f = 0.35$ THz, especially for lower transmitted power values. This is consistent with the findings reported in Figure (3.1) of [60] which indicate that molecular attenuation due to water vapor becomes more significant in the region of 0.35 THz in comparison with the region of 0.3 THz. Consequently, although it appears that increasing the frequency of the carrier wave could have a positive contribution to establish THz links of a higher available bandwidth, particular attention should be given to the molecular attenuation due to water vapor.

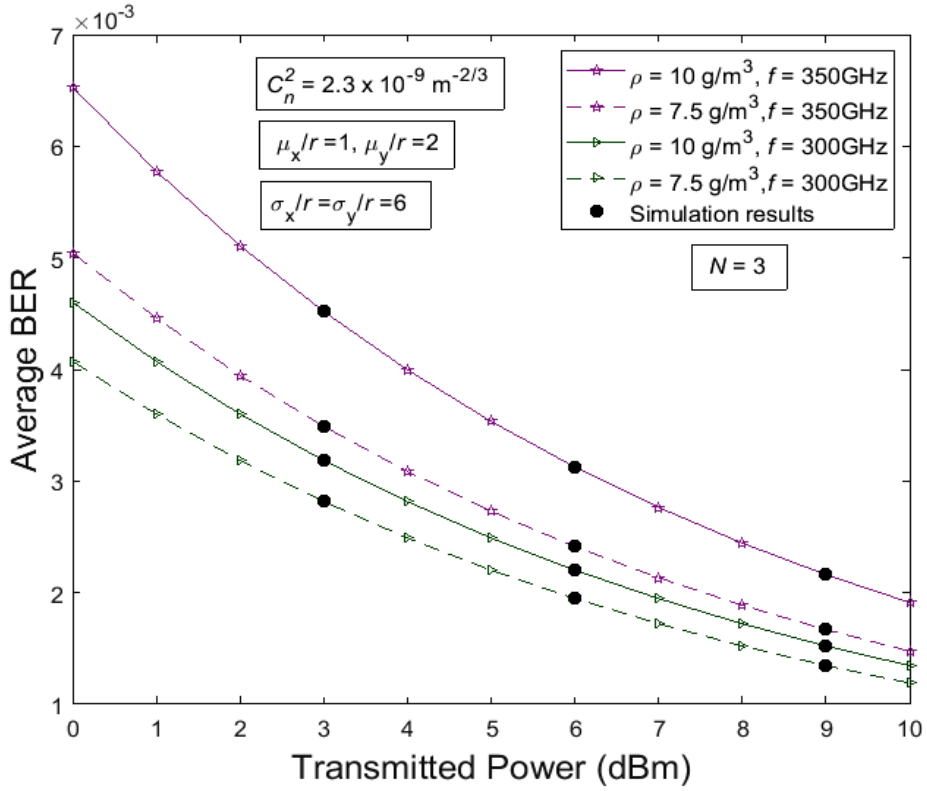


**Figure 4.** ABER vs. transmitted power for a triple-hop THz link configuration under strong turbulence, moderate-to-high water vapor concentrations, different operational frequencies and strong NZB pointing errors.

Figure 5 shows the ABER evolution for single-hop, dual-hop, triple-hop or quad-hop LOS THz link configurations over a wide range of transmitted power through strong atmospheric turbulence, strong NZB pointing errors, rain along with moderate-to-high air humidity conditions. Thus, in view of the above, Figure 5 depicts the worst-case scenario for each topology. In order to address this issue, we have selected the high gain transceiver pair of $G = 70$ dBi along with the operation frequency $f = 0.3$ THz which is more resilient to humid air than $f = 0.35$ THz, as mentioned above. The results demonstrate that, under these adverse circumstances, it may not be wise to extend the end-to-end link length beyond two or three hops, especially for low transmitted power values and high ABER performance demands.

Figure 6 visualizes the ABER evolution for dual-hop or quad-hop LOS THz link configurations with different $L$-PAM modulation schemes over a wide range of transmitted power through strong atmospheric turbulence, weak NZB pointing errors, rain and moderate air humidity conditions. The ABER performance comparison between dual-hop configurations indicates that 2-PAM, which is a special case equivalent to OOK, outperforms 8-PAM. Nevertheless, considering that 8-PAM is more bandwidth-effective than OOK, it is highlighted that especially for higher transmitted power values, the selection of 8-PAM instead of OOK seems to be reasonable at the expense of an acceptable ABER increase for very high

bandwidth demanding applications. Additionally, the ABER performance comparison between quad-hop configurations indicates that, especially for lower transmitted power values, 8-PAM outperforms 16-PAM. Thus, the number of symbols to be transmitted should be increased with caution.

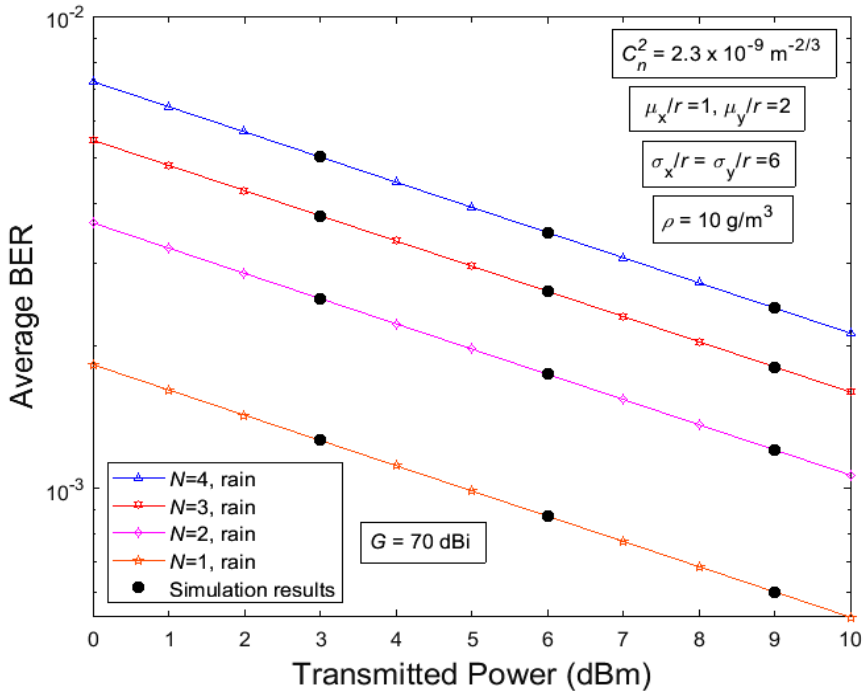


**Figure 5.** ABER vs. transmitted power for single-hop and multiple-hop THz link configurations under strong turbulence, rain, high water vapor concentration and strong NZB pointing errors.

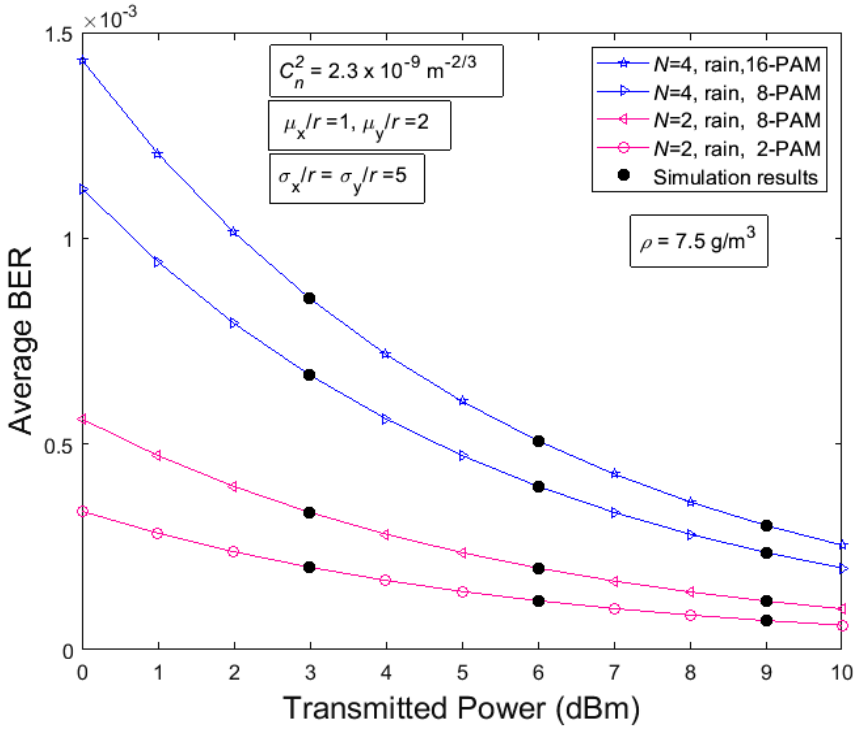


**Figure 6.** ABER vs. transmitted power for dual-hop and quad-hop THz link configurations with 2-, 8- or 16-PAM modulation formats under strong turbulence, rain, moderate water vapor concentration and weak NZB pointing errors.

## 5. Discussion

Single-hop and multi-hop LOS THz link configurations were investigated through weak-to-strong atmospheric turbulent channels under the presence of moderate-to-high air humidity, free-space path loss, different weather conditions including clear sky, rain, or fog along with weak-to-strong generalized stochastic pointing errors. The stochastic effects of turbulence-induced scintillations and generalized pointing error misalignment-induced fading have been described through the appropriate statistical distribution models, i.e., Gamma–Gamma and Beckmann distribution models, respectively. Under these circumstances, the joint impact of all the above major effects has been evaluated in the open THz literature for the first time. Furthermore, the potential of establishing multi-hop THz links to increase the total coverage area has been first investigated. In this context, an outage performance analysis has been performed in terms of the critical ABER metric. Thus, novel closed-form ABER expressions that jointly incorporate the impact of atmospheric turbulence, pointing errors with or without boresight, molecular attenuation due to water vapor, free space path loss, attenuation due to rain or fog droplets were derived. Additionally, the extracted closed-form ABER expressions include the impact of critical link parameters, such as the operation frequency, the transmitted power, the transceivers' antenna gain, the number of the implemented relay nodes along with the link length of each hop. By adjusting realistic values for each crucial parameter, their results demonstrate the feasibility of significantly extending the end-to-end THz propagation distance through the use of serially connected relay nodes in most of the examined scenarios. It is also worth noting that the obtained results for each specific effect are qualitatively consistent with the previously reported experimental and theoretical predictions in the open THz literature. Additionally, proper simulation results further validate the obtained ABER analytical results. In short, the proposed analysis may be a useful tool in the design of the emerging THz links intended to cover longer propagation distances.

## 6. Conclusions

The use of THz band provides a prime alternative for establishing high-speed wireless communication links. In this context, the proposed LOS multi-hop DF relaying THz system has been proved to significantly extend the total THz coverage area by achieving encouraging results in terms of the ABER metric. According to our findings, the most detrimental effect which mitigates the ABER performance is humid air by means of molecular attenuation due to water vapor along the propagation path, especially along with rain conditions. Contrary to FSOs, which are highly vulnerable to fog and atmospheric turbulence and to a lesser extent to rain and humid air, our findings validate that fog, along with atmospheric turbulence, are not the most important ABER degrading factors for THz links. The latter therefore gives rise to the development of hybrid FSO/THz links which will be able to efficiently co-operate in both rain and fog conditions along with humid air turbulent channels. Another important outcome of this paper is that the boresight component should be considered on the estimation of stochastic misalignment-induced fading which can unavoidably but significantly further degrade the ABER performance of THz links. Finally, the feasibility of utilizing higher order $L$-PAM modulation formats in the THz band has been verified, which enhances the total spectral efficiency but at a reasonable and acceptable expense of ABER performance degradation.

**Author Contributions:** Conceptualization, G.K.V., K.A. and H.E.N.; Methodology, G.K.V., K.A. and H.E.N.; Software, G.K.V. and K.A.; Validation, G.K.V., H.E.N. and K.A.; Investigation, G.K.V., H.E.N. and K.A.; Resources, G.K.V., K.A. and H.E.N.; Writing—original draft preparation, G.K.V.; Writing—review and editing, G.K.V. and H.E.N.; Supervision, G.K.V., K.A. and H.E.N.; Funding acquisition, G.K.V., K.A. and H.E.N. All authors have read and agreed to the published version of the manuscript.

**Funding:** This research was funded by Ajman University, grant number 2021-IRG-ENIT-10.

**Acknowledgments:** The authors acknowledge funding from Ajman University under grant agreement 2021-IRG-ENIT-10.

**Conflicts of Interest:** The authors declare no conflict of interest.

## References


1. Ghassemlooy, Z.; Arnon, S.; Uysal, M.; Xu, Z.; Cheng, J. Emerging optical wireless communications-advances and challenges. *IEEE J. Sel. Areas Commun.* **2015**, *33*, 1738–1749. [CrossRef]
2. Varotsos, G.K.; Nistazakis, H.E.; Petkovic, M.I.; Djordjevic, G.T.; Tombras, G.S. SIMO optical wireless links with nonzero boresight pointing errors over M modeled turbulence channels. *Opt. Commun.* **2017**, *403*, 391–400. [CrossRef]
3. Varotsos, G.K.; Nistazakis, H.E.; Aidinis, K.; Jaber, F.; Rahman, K.K. Transdermal Optical Wireless Links with Multiple Receivers in the Presence of Skin-Induced Attenuation and Pointing Errors. *Computation* **2019**, *7*, 33. [CrossRef]
4. Wang, X.; Kong, L.; Kong, F.; Qiu, F.; Xia, M.; Arnon, S.; Chen, G. Millimeter wave communication: A comprehensive survey. *IEEE Commun. Surv. Tutor.* **2018**, *20*, 1616–1653. [CrossRef]
5. Shawon, M.E.; Chowdhury, M.Z.; Hossen, M.B.; Ahmed, M.F.; Jang, Y.M. Rain Attenuation Characterization for 6G Terahertz Wireless Communication. In Proceedings of the 2021 International Conference on Artificial Intelligence in Information and Communication (ICAIIC), Jeju Island, Korea, 20–23 April 2021; pp. 3535–3538.
6. Seeds, A.J.; Shams, H.; Fice, M.J.; Renaud, C.C. Terahertz photonics for wireless communications. *J. Light. Technol.* **2015**, *33*, 579–587. [CrossRef]
7. Akyildiz, I.F.; Jornet, J.M.; Han, C. Terahertz band: Next frontier for wireless communications. *Phys. Commun.* **2014**, *12*, 16–32. [CrossRef]
8. Federici, J.F.; Ma, J.; Moeller, L. Review of weather impact on outdoor terahertz wireless communication links. *Nano Commun. Netw.* **2016**, *10*, 13–26. [CrossRef]
9. Chowdhury, M.Z.; Shahjalal, M.; Ahmed, S.; Jang, Y.M. 6G wireless communication systems: Applications, requirements, technologies, challenges, and research directions. *IEEE Open J. Commun. Soc.* **2020**, *1*, 957–975. [CrossRef]
10. Federici, J.; Moeller, L. Review of terahertz and subterahertz wireless communications. *J. Appl. Phys.* **2010**, *107*, 111101. [CrossRef]
11. Su, K.; Moeller, L.; Barat, R.B.; Federici, J.F. Experimental comparison of terahertz and infrared data signal attenuation in dust clouds. *JOSA A* **2012**, *29*, 2360–2366. [CrossRef]
12. Su, K.; Moeller, L.; Barat, R.B.; Federici, J.F. Experimental comparison of performance degradation from terahertz and infrared wireless links in fog. *JOSA A* **2012**, *29*, 179–184. [CrossRef] [PubMed]
13. Yang, Y.; Mandehgar, M.; Grischkowsky, D.R. Broadband THz signals propagate through dense fog. *IEEE Photon. Technol. Lett.* **2014**, *27*, 383–386. [CrossRef]
14. Ma, J.; Moeller, L.; Federici, J.F. Experimental comparison of terahertz and infrared signaling in controlled atmospheric turbulence. *J. Infrared Millim. Terahertz Waves* **2015**, *36*, 130–143. [CrossRef]
15. Ma, J.; Vorrius, F.; Lamb, L.; Moeller, L.; Federici, J.F. Experimental comparison of terahertz and infrared signaling in laboratory-controlled rain. *J. Infrared Millim. Terahertz Waves* **2015**, *36*, 856–865. [CrossRef]
16. Ma, J.; Vorrius, F.; Lamb, L.; Moeller, L.; Federici, J.F. Comparison of experimental and theoretical determined terahertz attenuation in controlled rain. *J. Infrared Millim. Terahertz Waves* **2015**, *36*, 1195–1202. [CrossRef]
17. Ishii, S.; Sayama, S.; Kamei, T. Measurement of rain attenuation in terahertz wave range. *Wirel. Eng. Technol.* **2011**, *2*, 119–124. [CrossRef]
18. Yang, Y.; Mandehgar, M.; Grischkowsky, D. Determination of the water vapor continuum absorption by THz-TDS and molecular response theory. *Opt. Express* **2014**, *22*, 4388–4403. [CrossRef]
19. Taherkhani, M.; Kashani, Z.G.; Sadeghzadeh, R.A. On the performance of THz wireless LOS links through random turbulence channels. *Nano Commun. Netw.* **2020**, *23*, 100282. [CrossRef]
20. Chatzidiamantis, N.D.; Sandalidis, H.G.; Karagiannidis, G.K.; Matthaiou, M. Inverse Gaussian modeling of turbulence-induced fading in free-space optical systems. *J. Light. Technol.* **2011**, *29*, 1590–1596. [CrossRef]
21. Varotsos, G.K.; Nistazakis, H.E.; Stassinakis, A.N.; Volos, C.K.; Christofilakis, V.; Tombras, G.S. Mixed Topology of DF Relayed Terrestrial Optical Wireless Links with Generalized Pointing Errors over Turbulence Channels. *Technologies* **2018**, *6*, 121. [CrossRef]
22. Varotsos, G.K.; Nistazakis, H.E.; Tombras, G.S. OFDM RoFSO Links with Relays Over Turbulence Channels and Nonzero Boresight Pointing Errors. *J. Commun.* **2017**, *12*, 644. [CrossRef]
23. Varotsos, G.K.; Nistazakis, H.E.; Gappmair, W.; Sandalidis, H.G.; Tombras, G.S. DF relayed subcarrier FSO links over Malaga turbulence channels with phase noise and non-zero boresight pointing errors. *Appl. Sci.* **2018**, *8*, 664. [CrossRef]
24. Farid, A.A.; Hranilovic, S. Outage capacity optimization for free space optical links with pointing errors. *IEEE/OSA J. Light. Technol.* **2007**, *25*, 1702–1710. [CrossRef]
25. Tsiftsis, T.A.; Sandalidis, H.G.; Karagiannidis, G.K.; Uysal, M. Optical wireless links with spatial diversity over strong atmospheric turbulence channels. *IEEE Trans.Wirel. Commun.* **2009**, *8*, 951–957. [CrossRef]
26. Gappmair, W.; Hranilovic, S.; Leitgeb, E. Performance of PPM on terrestrial FSO links with turbulence and pointing errors. *IEEE Commun. Lett.* **2010**, *14*, 468–470. [CrossRef]

27. Boulogeorgos, A.A.A.; Papasotiriou, E.N.; Alexiou, A. Analytical performance assessment of THz wireless systems. *IEEE Access* **2019**, *7*, 11436–11453. [CrossRef]
28. Yang, F.; Cheng, J.; Tsiftsis, T.A. Free-space optical communication with nonzero boresight pointing errors. *IEEE Trans. Commun.* **2014**, *62*, 713–725. [CrossRef]
29. Yang, Y.; Shutler, A.; Grischkowsky, D.J.O.E. Measurement of the transmission of the atmosphere from 0.2 to 2 THz. *Opt. Express* **2011**, *19*, 8830–8838. [CrossRef]
30. Nagatsuma, T.; Yoshimizu, Y.; Yasuda, Y.; Oogimoto, K.; Horiguchi, S.; Minamikata, Y.; Hisatake, S. 30-Gbit/s wireless transmission over 10 meters at 300 GHz. In Proceedings of the 2014 39th International Conference on Infrared, Millimeter, and Terahertz waves (IRMMW-THz), Tucson, AZ, USA, 14–19 September 2014; pp. 1–2.
31. Kim, G.R.; Jeon, T.I.; Grischkowsky, D. 910-m propagation of THz ps pulses through the atmosphere. *Opt. Express* **2017**, *25*, 25422–25434. [CrossRef]
32. Kokkoniemi, J.; Lehtomäki, J.; Juntti, M. Simplified molecular absorption loss model for 275–400 gigahertz frequency band. In Proceedings of the 12th European Conference on Antennas and Propagation (EuCAP 2018), London, UK, 9–13 April 2018; pp. 1–5.
33. Boulogeorgos, A.A.A.; Papasotiriou, E.N.; Kokkoniemi, J.; Lehtomäki, J.; Alexiou, A.; Juntti, M. Performance evaluation of THz wireless systems operating in 275–400 GHz band. In Proceedings of the 2018 IEEE 87th Vehicular Technology Conference (VTC Spring), Porto, Portugal, 3–6 June 2018; pp. 1–5.
34. Fiorino, S.T.; Bartell, R.J.; Krizo, M.J.; Marek, S.L.; Bohn, M.J.; Randall, R.M.; Cusumano, S.J. A computational tool for evaluating THz imaging performance in brownout or whiteout conditions at land sites throughout the world. In *Atmospheric Propagation VI*; SPIE: Orlando, FL, USA, 2009; Volume 7324, pp. 308–319.
35. Kokkonen, M.; Juttula, H.; Mäkynen, A.; Myllymäki, S.; Jantunen, H. The effect of drop shape, sensing volume and raindrop size statistics to the scattered field on 300 GHz. *IEEE Access* **2021**, *9*, 101381–101389. [CrossRef]
36. Moon, E.B.; Jeon, T.I.; Grischkowsky, D.R. Long-path THz-TDS atmospheric measurements between buildings. *IEEE Trans. Terahertz Sci. Technol.* **2015**, *5*, 742–750. [CrossRef]
37. Castro, C.; Elschner, R.; Merkle, T.; Schubert, C.; Freund, R. Long-range high-speed THz-wireless transmission in the 300 GHz band. In Proceedings of the 2020 Third International Workshop on Mobile Terahertz Systems (IWMTS), Essen, Germany, 1–2 July 2020; pp. 1–4.
38. Ma, J.; Moeller, L.; Federici, J. Terahertz performance in atmospheric turbulence. In Proceedings of the 2014 39th International Conference on Infrared, Millimeter, and Terahertz Waves (IRMMW-THz), Tucson, AZ, USA, 14–19 September 2014; pp. 1–4.
39. Bao, L.; Zhao, H.; Zheng, G.; Ren, X. Scintillation of THz transmission by atmospheric turbulence near the ground. In Proceedings of the 2012 IEEE Fifth International Conference on Advanced Computational Intelligence (ICACI), Nanjing, China, 18–20 October 2012; pp. 932–936.
40. Taherkhani, M.; Sadeghzadeh, R.A.; Kashani, Z.G. Attenuation analysis of THz/IR waves under different turbulence conditions using gamma-gamma model. In Proceedings of the Electrical Engineering (ICEE), Iranian Conference on, Sadjad University of Technology, Mashhad, Iran, 8–10 May 2018; pp. 424–428.
41. Varotsos, G.K.; Chatzikontis, E.V.; Kapotis, E.; Nistazakis, H.E.; Aidinis, K.; Christofilakis, V. THz Links Performance Study for Gamma Turbulence Links with Path Loss and Pointing Errors. In Proceedings of the 2022 11th International Conference on Modern Circuits and Systems Technologies (MOCAST), Bremen, Germany, 8–10 June 2022; pp. 1–4.
42. Priebe, S.; Jacob, M.; Kürner, T. The impact of antenna directivities on THz indoor channel characteristics. In Proceedings of the 2012 6th European Conference on Antennas and Propagation (EUCAP), Prague, Czech Republic, 26–30 March 2012; pp. 478–482.
43. Ekti, A.R.; Boyaci, A.; Alparslan, A.; Ünal, İ.; Yarkan, S.; Görçin, A.; Arslan, H.; Uysal, M. Statistical modeling of propagation channels for terahertz band. In Proceedings of the 2017 IEEE Conference on Standards for Communications and Networking (CSCN), Helsinki, Finland, 18–20 September 2017; pp. 275–280.
44. Han, C.; Akyildiz, I.F. Three-dimensional end-to-end modeling and analysis for graphene-enabled terahertz band communications. *IEEE Trans. Veh. Technol.* **2016**, *66*, 5626–5634. [CrossRef]
45. Papasotiriou, E.N.; Boulogeorgos, A.A.A.; Alexiou, A. Performance analysis of THz wireless systems in the presence of antenna misalignment and phase noise. *IEEE Commun. Lett.* **2020**, *24*, 1211–1215. [CrossRef]
46. Kokkoniemi, J.; Boulogeorgos, A.A.A.; Aminu, M.; Lehtomäki, J.; Alexiou, A.; Juntti, M. Impact of beam misalignment on THz wireless systems. *Nano Commun. Netw.* **2020**, *24*, 100302. [CrossRef]
47. Rong, Z.; Leeson, M.S.; Higgins, M.D. Relay-assisted nanoscale communication in the THz band. *Micro Nano Lett.* **2017**, *12*, 373–376. [CrossRef]
48. Abbasi, Q.H.; Nasir, A.A.; Yang, K.; Qaraqe, K.A.; Alomainy, A. Cooperative in-vivo nano-network communication at terahertz frequencies. *IEEE Access* **2017**, *5*, 8642–8647. [CrossRef]
49. Samarasekera, A.C.J.; Shin, H. Outage probability for cooperative nano communication in the THz gap frequency range. *KSII Trans. Internet Inf. Syst.* **2017**, *11*, 102–122.
50. Boulogeorgos, A.A.A.; Alexiou, A. Outage probability analysis of THz relaying systems. In Proceedings of the 2020 IEEE 31st Annual International Symposium on Personal, Indoor and Mobile Radio Communications, London, UK, 31 August–3 September 2020; pp. 1–7.

51. Stratidakis, G.; Papasotiriou, E.N.; Konstantinis, H.; Boulogeorgos, A.A.A.; Alexiou, A. Relay-based blockage and antenna misalignment mitigation in THz wireless communications. In Proceedings of the 2020 2nd 6G Wireless Summit (6G SUMMIT), Levi, Finland, 17–20 March 2020; pp. 1–4.
52. Xia, Q.; Jornet, J.M. Multi-hop Relaying Distribution Strategies for Terahertz-band Communication Networks: A Cross-layer Analysis. *IEEE Trans. Wirel. Commun.* **2021**, *21*, 5075–5089. [CrossRef]
53. Li, S.; Yang, L. Performance analysis of dual-hop THz transmission systems over α-μ fading channels with pointing errors. *IEEE Internet Things J.* **2021**, *9*, 11772–11783. [CrossRef]
54. Bhardwaj, P.; Zafaruddin, S.M. Performance of dual-hop relaying for THz-RF wireless link. In Proceedings of the 2021 IEEE 93rd Vehicular Technology Conference (VTC2021-Spring), Helsinki, Finland, 25–28 April 2021; pp. 1–5.
55. Tsiftsis, T.A.; Sandalidis, H.G.; Karagiannidis, G.K.; Sagias, N.C. Multihop free-space optical communications over strong turbulence channels. In Proceedings of the 2006 IEEE International Conference on Communications, Istanbul, Turkey, 11–15 June 2006; Volume 6, pp. 2755–2759.
56. Safari, M.; Uysal, M. Relay-assisted free-space optical communication. *IEEE Trans. Wirel. Commun.* **2008**, *7*, 5441–5449. [CrossRef]
57. Sheng, M.; Jiang, P.; Hu, Q.; Su, Q.; Xie, X.X. End-to-end average BER analysis for multihop free-space optical communications with pointing errors. *J. Opt.* **2013**, *15*, 055408. [CrossRef]
58. Tang, X.; Wang, Z.; Xu, Z.; Ghassemlooy, Z. Multihop free-space optical communications over turbulence channels with pointing errors using heterodyne detection. *J. Light. Technol.* **2014**, *32*, 2597–2604. [CrossRef]
59. Siles, G.A.; Riera, J.M.; Garcia-del-Pino, P. Atmospheric attenuation in wireless communication systems at millimeter and THz frequencies [wireless corner]. *IEEE Antennas Propag. Mag.* **2015**, *57*, 48–61. [CrossRef]
60. Ippolito Jr, L.J. Attenuation by Atmospheric Gases. In *Radiowave Propagation in Satellite Communications*; Van Nostrand Reinhold Co.: New York, NY, USA, 1986; pp. 25–37.
61. Ghassemlooy, Z.; Popoola, W.O. Terrestrial free-space optical communications. In *Mobile and Wireless Communications*; InTech: London, UK, 2010; pp. 355–392.
62. Popoola, W.O.; Ghassemlooy, Z.; Ahmadi, V. Performance of sub-carrier modulated free-space optical communication link in negative exponential atmospheric turbulence environment. *Int. J. Auton. Adapt. Commun. Syst.* **2008**, *1*, 342–355. [CrossRef]
63. Varotsos, G.K.; Nistazakis, H.E.; Volos, C.K.; Tombras, G.S. FSO links with diversity pointing errors and temporal broadening of the pulses over weak to strong atmospheric turbulence channels. *Optik* **2016**, *127*, 3402–3409. [CrossRef]
64. Ghassemlooy, Z.; Popoola, W.O.; Leitgeb, E. Free-space optical communication using subcarrier modulation in gamma-gamma atmospheric turbulence. In Proceedings of the 2007 9th International Conference on Transparent Optical Networks, Rome, Italy, 1–5 July 2007; Volume 3, pp. 156–160.
65. Al-Habash, A.; Andrews, L.C.; Phillips, R.L. Mathematical model for the irradiance probability density function of a laser beam propagating through turbulent media. *Opt. Eng.* **2001**, *40*, 1554–1562. [CrossRef]
66. Gradshteyn, I.S.; Ryzhik, I.M. *Table of Integrals, Series, and Products*, 6th ed.; Academic Press, Inc.: New York, NY, USA, 2000.
67. Varotsos, G.K.; Nistazakis, H.E.; Stassinakis, A.N.; Tombras, G.S.; Christofilakis, V.; Volos, C.K. Outage performance of mixed, parallel and serial DF relayed FSO links over weak turbulence channels with nonzero boresight pointing errors. In Proceedings of the 2018 7th International Conference on Modern Circuits and Systems Technologies (MOCAST), Thessaloniki, Greece, 7–9 May 2018; pp. 1–4.
68. Nistazakis, H.E.; Tombras, G.S. On the use of wavelength and time diversity in optical wireless communication systems over gamma–gamma turbulence channels. *Opt. Laser Technol.* **2012**, *44*, 2088–2094. [CrossRef]
69. Boluda-Ruiz, R.; García-Zambrana, A.; Castillo-Vázquez, C.; Castillo-Vázquez, B. Novel approximation of misalignment fading modeled by Beckmann distribution on free-space optical links. *Opt. Express* **2016**, *24*, 22635–22649. [CrossRef]
70. Abramovitz, M.; Stegun, I.A. *Handbook of Mathematical Functions with Formulas, Graphs, and Mathematical Tables*, 9th ed.; Dover: New York, NY, USA, 1972.
71. The Wolfram Functions Site. 2008. Available online: https://functions.wolfram.com (accessed on 13 July 2022).
72. Adamchik, V.S.; Marichev, O.I. The algorithm for calculating integrals of hypergeometric type functions and its realization in REDUCE system. In Proceedings of the International Symposium on Symbolic and Algebraic Computation, Tokyo, Japan, 1 July 1990; pp. 212–224.
73. Morgado, E.; Mora-Jimenez, I.; Vinagre, J.J.; Ramos, J.; Caamano, A.J. End-to-end average BER in multihop wireless networks over fading channels. *IEEE Trans. Wirel. Commun.* **2010**, *9*, 2478–2487. [CrossRef]
74. Androutsos, N.A.; Nistazakis, H.E.; Petkovic, M.I.; Djordjevic, G.T.; Stassinakis, A.N.; Volos, C.K. Multi-hop DF relayed FSO links with various modulation formats emulated by a dual-hop scheme for strong turbulence conditions. *Optik* **2021**, *227*, 165972. [CrossRef]
75. Elganimi, T.Y. Studying the BER performance, power-and bandwidth-efficiency for FSO communication systems under various modulation schemes. In Proceeding of the 2013 IEEE Jordan Conference on Applied Electrical Engineering and Computing Technologies (AEECT), Amman, Jordan, 3–5 December 2013; pp. 1–6.
76. Varotsos, G.K.; Nistazakis, H.E.; Aidinis, K.; Jaber, F.; Nasor, M.; Rahman, K.M. On the Utilization of L-PAM Technique in Transdermal Optical Wireless Links with Stochastic Pointing Errors for ABER Performance Estimation. In Proceedings of the 2021 10th International Conference on Modern Circuits and Systems Technologies (MOCAST), Thessaloniki, Greece, 5–7 July 2021; pp. 1–4.

77. Wang, H.; Dong, X.; Yi, M.; Xue, F.; Liu, Y.; Liu, G. Terahertz high-gain offset reflector antennas using SiC and CFRP material. *IEEE Trans. Antennas Propag.* **2017**, *65*, 4443–4451. [CrossRef]
78. Awan, M.S.; Capsoni, C.; Leitgeb, E.; Nebuloni, R.; Nadeem, F.; Khan, M.S. FSO-relevant new measurement results under moderate continental fog conditions at graz and milan. In Proceedings of the 2008 4th Advanced Satellite Mobile Systems, Bologna, Italy, 26–28 August 2008; pp. 116–121.